Applied Mathematics and Mechanics
(English Edition, Vol. 19, No. 8, Aug. 1998)

Published by SU,
Shanghai, China

MILU-CG METHOD AND THE NUMERICAL STUDY ON THE FLOW AROUND A ROTATING CIRCULAR CYLINDER*

Ling Guoping (凌国平)[1] Ling Guocan (凌国灿)[2]

(Received Jan. 31, 1996; Revised Dec. 29, 1997; Communicated by Bian Yinggui)

Abstract

A hybrid finite difference method and vortex method (HDV), which is based on domain decomposition and proposed by the authors (1992), is improved by using a modified incomplete LU decomposition conjugate gradient method (MILU-CG), and a high order implicit difference algorithm. The flow around a rotating circular cylinder at Reynolds number $R_e=1000$, 200 and the angular to rectilinear speed ratio $\alpha \in (0.5, 3.25)$ is studied numerically. The long-time full developed features about the variations of the vortex patterns in the wake, and drag, lift forces on the cylinder are given. The calculated streamline contours agreed well with the experimental visualized flow pictures. The existence of critical states and the vortex patterns at the states are given for the first time. The maximum lift to drag force ratio can be obtained nearby the critical states.

Key words rotating circular cylinder, vortex pattern, finite difference method, vortex method, preconditioned conjugate gradient method, incomplete LU decomposition

I. Introduction

The flow around a rotating circular cylinder is a complex unsteady one. It includes many complicated flow phenomena such as the unsteady boundary layer separation, the generation and shedding of vortices and the interaction with wakes etc.. The rotation of a circular cylinder around its axis will decrease and suppress the flow separation and vortex shedding on one side of the cylinder, while increasing and developing on another side. A transverse lift force will act on the cylinder, and this phenomenon is called the Magnus effect. The most important parameter for the case is the angular to rectilinear speed ratio $\alpha(= \Omega a/U_\infty$, where Ω is the angular speed of the cylinder, a the radius of the cylinder, U_∞ the ambient flow velocity at infinity). The variation of $\dot{a}$ will effectively change the vortex patterns in the wake, so the drag and lift forces on the cylinder. It is one of the important subjects in flow control

* Project supported by the Natural Science Foundations of Province Jiangsu of China and the Laboratory for Nonlinear Mechanics, Institute of Mechanics, Academia Sinica

[1] Department of Mathematics, Suzhou University, Suzhou 215006, P. R. China

[2] Institute of Mechanics, Academia Sinica, Beijing 100080, P. R. China

research currently to well know the effect of cylinder rotation, to which great attentions are paid by many fluid mechanists in the world.

The early research works were only for smaller a and lower Re flow regions. Since 80s, a series of experimental[1]~[3] and numerical[3]~[6] studies has been carried out for some larger a and higher Re flow regions. But, trere are some issues of whether the vortex shedding will be depressed and disappear completely, while the flow is approaching steadily. The article [5] indicates that rotation does not suppress vortex shedding even for Re=200, a=3.25. After the first main vortex (the initial starting vortex), there are still the second and third (and so on) vortices shed from the same side of the cylinder (called the single side vortex shedding). This is contradictory to the experimental results of [1]. [1] indicates that after the first main vortex, the flow is tending to steady and the vortex shedding disappears completely then. Recently a systematical study on the flow around a rotating circular cylinder for Re=100, $\alpha \in (0.5,6)$ is done in [7]. Its results support the conclusions of [1], but does not give more details about the flow characters at the critical states.

The authors proposed (1992) a hybrid finite difference and vortex method (HDV), which was based on domain decomposition, and applied it to calculating the impulsively started flow[8, 9] and oscillating flow[10] around a circular cylinder successfully. With the increasing flow complexity, some more effective, stable and accurate computational methods must be developed. Besides finer grids, the higher order (greater than 2) implicit difference algorithm should be adopted. It will produce a kind of large broad band (more than 3 diagonals) sparse matrix equations. For such equations, some traditionally used methods in CFD, like the ADI method or SIP method etc., are not valid or efficient any longer. An advanced, effective conjugate gradient method with modified incomplete LU decomposition as preconditioner (MILU-CG) is adopted insteadly. It can simultaneously fast solve the broad band matrix equations and doesn't need any alternate directional iteration process. It belongs to the most optimized kind of updated algorithms in the large scale scientific and engineering computations[11]. The MILU-CG method combined with the modified HDV method is used for calculating the flow around a rotating circular cylinder at Re=1000, 200, $\alpha \in (0.5,3.25)$ for investigating the variation rules of vortex patterns and forces in long time period from start to full developed. The calculated streamline contours are agreed well with the experimental visualized flow pictures. The characters of vortex patterns at the critical states are given for the first time. The maximum lift to drag force ratio is discovered to be obtained nearby the states.

II. Mathematical Model

The flow is assumed to be viscous and incompressible, with a uniform velocity U_∞ at infinity in the x-direction. A circular cylinder of radius a rotates in the counterclockwise direction with angular velocity Ω. The origin of the reference (r,θ) coincides with the centre of the cylinder. In order to make the meshes denser in the vicinity of the cylinder surface, we introduce a log-polar coordinate system, i. e. $r = \exp(2\pi\xi)$, $\theta = 2\pi\eta$.

The dimensionless governing equations of the flow, in the form of vorticity(ω) and stream function (Ψ), are

$$E\frac{\partial\omega}{\partial t} + \frac{\partial}{\partial\xi}(U\omega) + \frac{\partial}{\partial\eta}(V\omega) = \frac{2}{Re}\nabla^2\omega \tag{2.1}$$

$$\nabla^2\Psi = -E\omega \tag{2.2}$$

where

$$\nabla^2 = \frac{\partial^2}{\partial \xi^2} + \frac{\partial^2}{\partial \eta^2}, \quad E = 4\pi^2 e^{4\pi\xi}, \quad Re = \frac{2U_\infty a}{\nu}$$

$$U = \frac{\partial \Psi}{\partial \eta} = E^{1/2} V_r, \quad V = -\frac{\partial \Psi}{\partial \xi} = E^{1/2} V_\theta$$

On the cylinder surface ($\xi = 0$) the non-slip condition of impermeable wall must be satisfied, i. e.

$$\left.\begin{aligned} &\Psi = 0, \ \frac{\partial \Psi}{\partial \xi} = -E^{1/2}\alpha \\ &\omega = -\frac{1}{E}\frac{\partial^2 \Psi}{\partial \xi^2} \end{aligned}\right\} \quad , \quad \xi = 0 \tag{2.3}$$

and at infinity the influence of rotation on the flow field can be neglected, i. e.

$$\left.\begin{aligned} &\frac{\partial \Psi}{\partial \xi} = E^{1/2}\sin(2\pi\eta) \\ &\frac{\partial \omega}{\partial \xi} = 0 \end{aligned}\right\} \quad , \quad \xi \to \infty \tag{2.4}$$

The periodical condition is

$$\Psi|_{\eta=0} = \Psi|_{\eta=1}, \quad \omega|_{\eta=0} = \omega|_{\eta=1} \tag{2.5}$$

and the initial condition is

$$\omega|_{t=0} = 0, \qquad \xi > 0 \tag{2.6}$$

Having got the vorticity distributions in the field from equations (2.1)~(2.6), we can deduce the distributions of the pressure and shear stress on the cylinder surface, as well as the drag and lift force coefficients, C_d and C_l,

$$\left.\begin{aligned} C_d &= \frac{2}{Re}\int_0^1 \left(\frac{\partial \omega}{\partial \xi} - 2\pi\omega\right)\Big|_{\xi=0} \sin(2\pi\eta)\, d\eta \\ C_l &= \frac{2}{Re}\int_0^1 \left(2\pi\omega - \frac{\partial \omega}{\partial \xi}\right)\Big|_{\xi=0} \cos(2\pi\eta)\, d\eta \end{aligned}\right\} \tag{2.7}$$

III. Numerical Methods

The basic idea of our numerical model is of the hybrid finite difference and vortex method (HDV), which is based on domain decomposition and proposed by the authors (1992), and some improvements are made in the difference algorithm and solver.

The flow field is divided into two regions, the inner region is immediately close to the cylinder surface, and the outer one covering the rest of the field. A finite difference method and a vortex method are used for calculating the flows in the inner region and the outer one respectively. The flows in the two regions are coupled through the interface.

For the convection term of the vorticity transport equation (2.1), a three order eccentric difference scheme is adopted. For example, the discrete form of the term $\partial(U\omega)/\partial\xi$ is

$$\begin{cases} ((U\omega)_{i+2,j} - 2(U\omega)_{i+1,j} + 9(U\omega)_{i,j} \\ \quad - 10(U\omega)_{i-1,j} + 2(U\omega)_{i-2,j})/6\Delta\xi & U_{i,j} > 0 \end{cases}$$

$$\frac{\partial}{\partial \xi}(U\omega) = \begin{cases} (-2(U\omega)_{i+2,j} + 10(U\omega)_{i+1,j} - 9(U\omega)_{i,j} \\ \quad + 2(U\omega)_{i-1,j} - (U\omega)_{i-2,j})/6\Delta\xi & U_{i,j} < 0 \end{cases}$$

For the viscous term in equation (2.1) and for the equation (2.2), a two order centrical difference scheme is used. The difference form for time forward march is implicit. So a nine and a five diagonal matrix equations will be produced. These matrix equations are solved by an advanced conjugate gradient method with modified incomplete LU decomposition as preconditioner (MILU-CG).

The preconditioned conjugate gradient method (PCG) is a kind of the best effective algorithms for solving such a large broad band sparse matrix equation $Ax=b$[11]. Its efficiency depends on the selection of preconditioner. A good selection of preconditioner is to desigh a matrix M, which must satisfy that, (1) the inverse matrix of M can be easily obtained, (2) the condition number of $M^{-1}A$ should be much less than of A. The procedure of PCG is as follows:

$X := X^0$

$g := AX - b;\ h := M^{-1}g$

$d := -h;\ \delta_0 := g^T h$

if $\delta_0 \leqslant \varepsilon$ then stop

R : continue

$h := Ad$

$\tau := \delta_0/(d^T h)$

$X := X + \tau d$

$g := g + \tau h$

$h := M^{-1}g$

$\delta_1 := g^T h$

if $\delta_1 \leqslant \varepsilon$ then stop

$\beta := \delta_1/\delta_0;\ \delta_0 := \delta_1$

$d := -h + \beta d$

goto R

One of the popular preconditioners is the incomplete LU decomposition (ILU). A subscript set $S_A = \{(i,j): a_{ij} \neq 0\}$ is defined. If a LU decomposition is only carried out to such a_{ij}, in which subscript belongs to S_A. This kind of decomposition is called the incomplete LU decomposition (ILU). Because of the spareness of A, the number of the elements in S_A is little. So the computation cost for LU is much less than for ILU. If the neglected term $-a_{ir}^r a_{rj}^r, (i,j) \in S_A$ is added to the main diagonal element, a more effective modified version of ILU, so called MILU, is formed. The procedure of MILU is as follows:

$A^0 := A$

for $r := 1$ to n do

begin

for $j \geqslant r$ and $(r,j) \in S_A$ do

$a_{rj}^r := a_{rj}^{r-1}$

for $i > r$ and $(i,r) \in S_A$ do

$a_{ir}^r := a_{ir}^{r-1}/a_{rr}^r$

for $i,j > r$ and $(i,r) \in S_A$ and $(r,j) \in S_A$ do

begin

$q := -a_{ir}^r a_{rj}^r$

if $(i,j) \in S_A$ then $a_{ij}^r := a_{ij}^{r-1} + q$

else $a_{ii}^r := a_{ii}^r + q$

end

end.

The $a_{ij}^n, (i,j) \in S_A$, gotten from the above, will be given to a lower triangular matrix L and a upper one U respectively. The inversion of the preconditioned matrix $M = LU$ can be obtained through a simple forward and backward return substitution procedure.

Within the same accuracy, the calculation speed for the modified incomplete LU decomposition conjugate gradient method (MILU-CG) is about six to eight times faster than that for the traditional line relaxation iteration (LSOR)[11, 12]. This advantage of speed will be more obvious with increasing the matrix scale and the complicity of the problem. So the latter is replaced by the former in the large matrix equation computations now.

The flow in the outer region is calculated by the Vortex-in-Cell method. To know the details of the calculation procedure, please refer to [8]~[10].

IV. Results

The flows around an impulsively started rotating circular cylinder for Re = 200, 1000 and $\alpha \in (0.5, 3.25)$ are simulated respectively. Fine grids are applied to the inner region, where the total number of grid nodes is 144 × 240, and the corresponding region on the physical plane is $a \leqslant r \leqslant 3a$, $0 \leqslant \theta \leqslant 2\pi$. Coarse grids are applied to the whole region, where the total number of grid nodes is 300 × 240, and the corresponding region on the physical plane is $a \leqslant r \leqslant 110a$, $0 \leqslant \theta \leqslant 2\pi$. The time step is $\Delta t = 0.01$. The calculation end time is $t = 80$.

In Fig. 1 the calculated streamline contours are compared with the experimental visualizations[1]~[3], [6] for $Re = 200$, (a) $\alpha = 0.5, t = 3$ and (b) $\alpha = 3.25, t = 5$. The good agreement between them has verified the accuracy of our numerical methods.

With the change of α, different vortex patterns will be presented in the wake of the cylinder.

Fig. 2 is of the streamline and vorticity contours at $t = 24$ for $Re = 200$, (a) $\alpha = 0.5$, and (b) $\alpha = 1$. The patterns in the both cases are of periodical alternate shedding votices from the upper and lower sides of the cylinder, just like the von Kármán vortex street in a stationary cylinder's wake. The streamline contours are periodically waved in large amplitudes, which central lines are deflected in the rotating direction with increasing α.

Fig. 3 is of the streamline and vorticity contours at $t = 24$, 45 for (a) Re = 1000, $\alpha = 3$, and (b) Re = 200, $\alpha = 3.25$. The development of vortex on the lower side is fully depressed. After the first main vortex is shed from the upper side, the flow is tending to steady. The shape of the

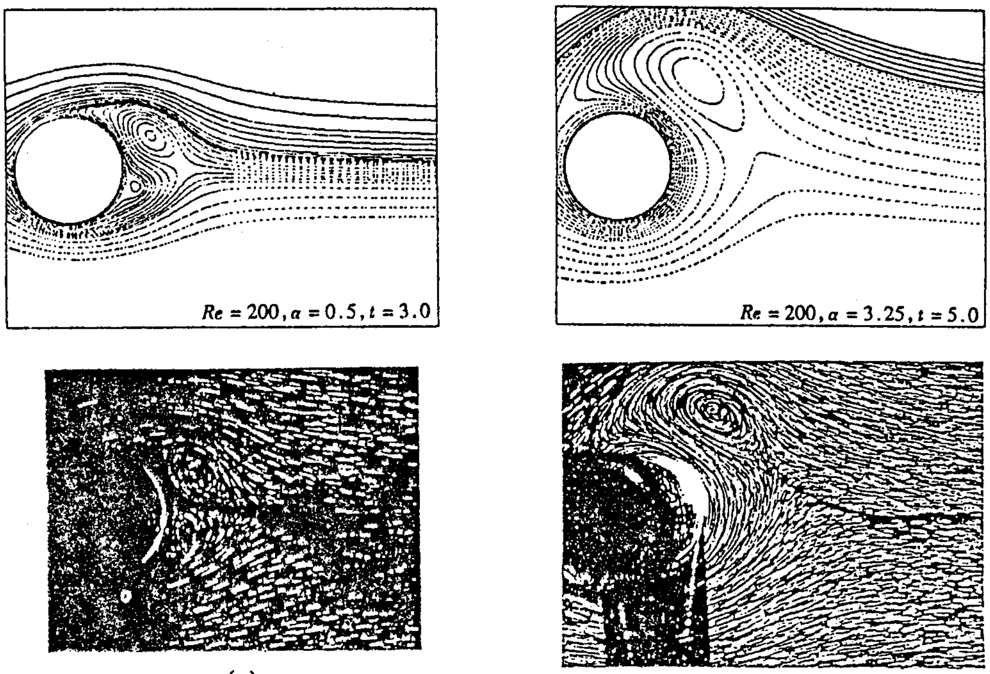

(a) (b)

Fig. 1 Comparison of the calculated streamline contour and experimental visualization for $R_e = 200$, (a) $\alpha = 0.5$, $t = 3$, (b) $\alpha = 3.25$, $t = 5$

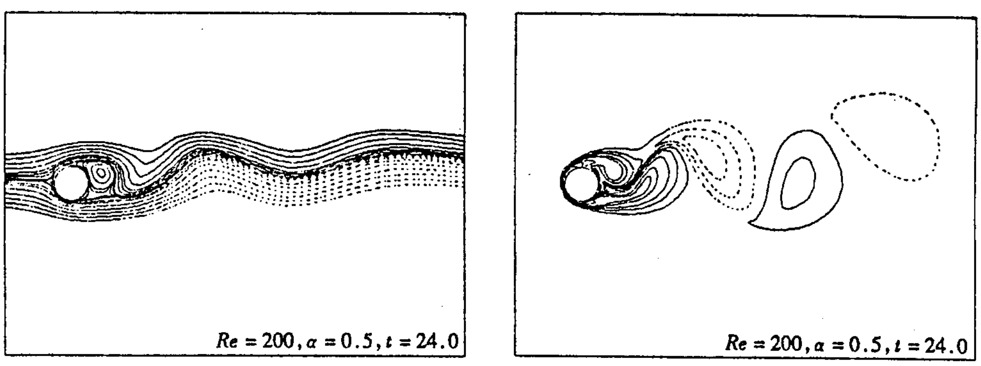

(a) $\alpha = 0.5$

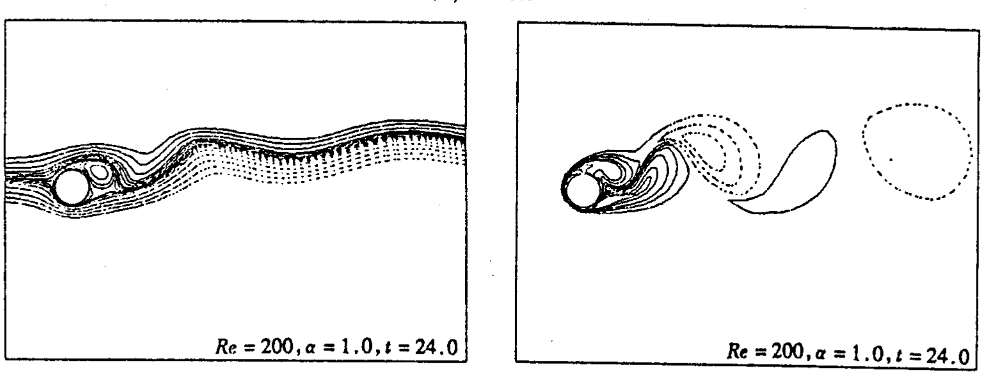

(b) $\alpha = 1$

Fig. 2 Streamline and vorticity contours at $t = 24$ for $R_e = 200$

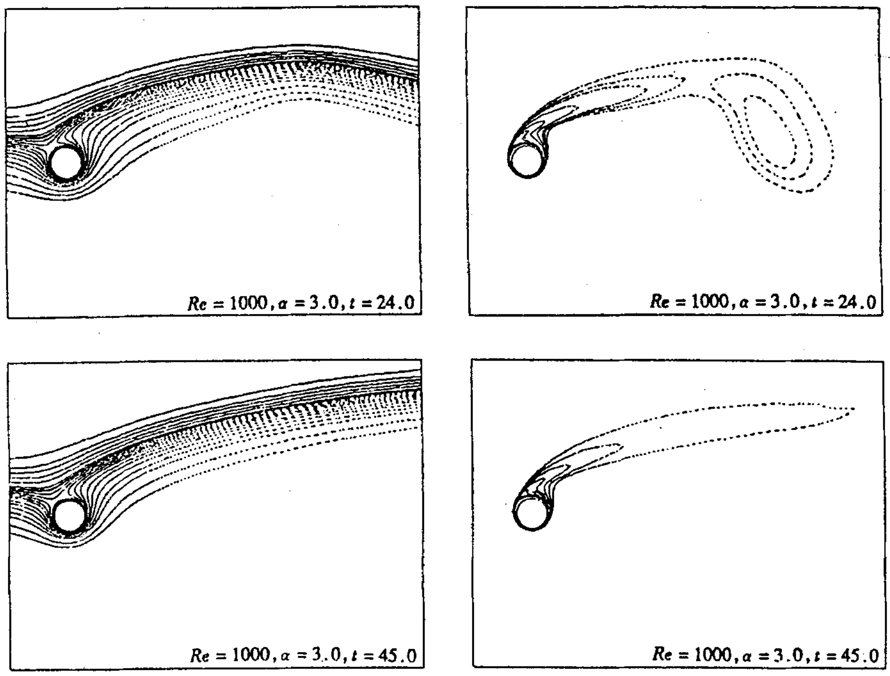

(a)

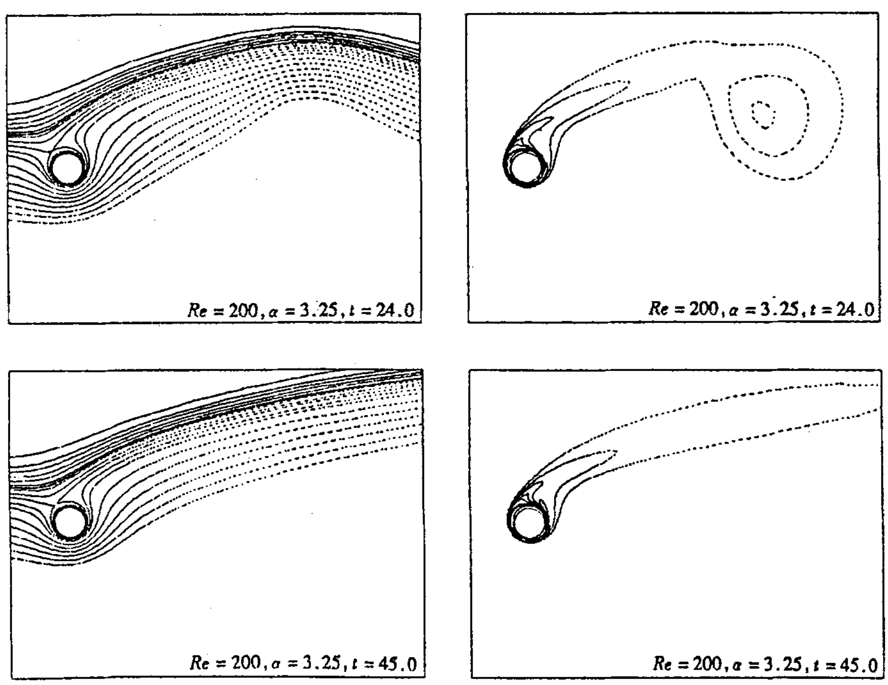

(b)

Fig. 3 Streamline and vorticity contours at $t=24, 45$ **for (a)** $R_e=1000$, $\alpha=3$, (b) $R_e=200$, $\alpha=3.25$.

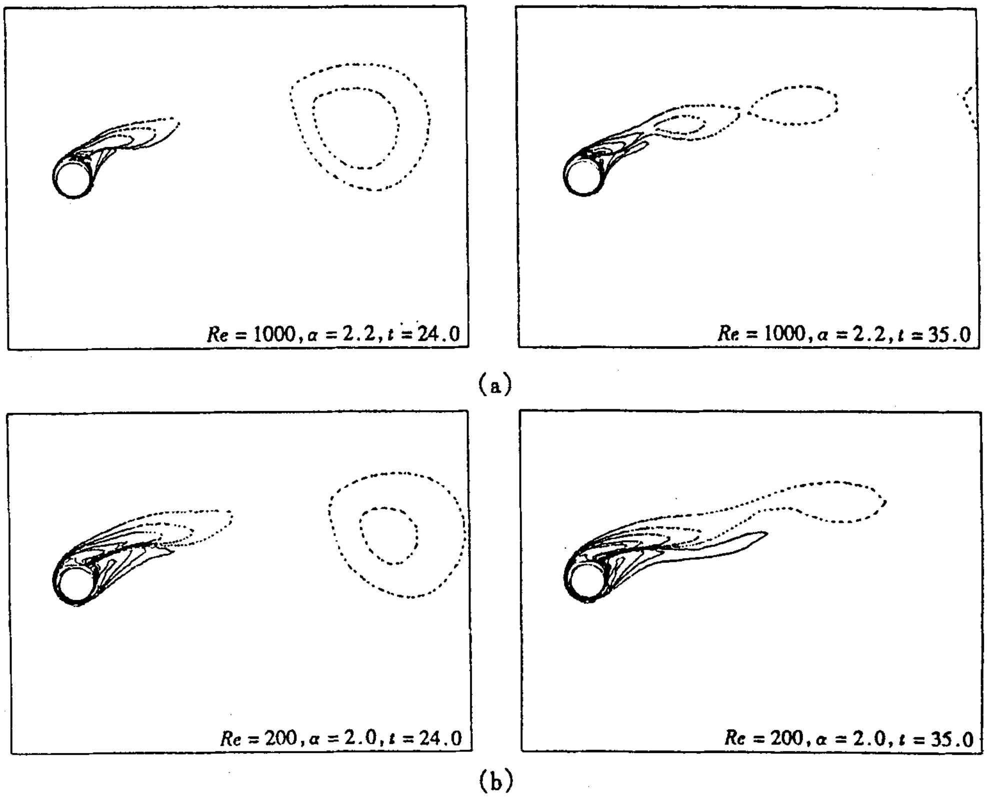

Fig. 4 Vorticity contours at critical states for (a) Re=1000, a=2.2, (b) Re=200, a=2.

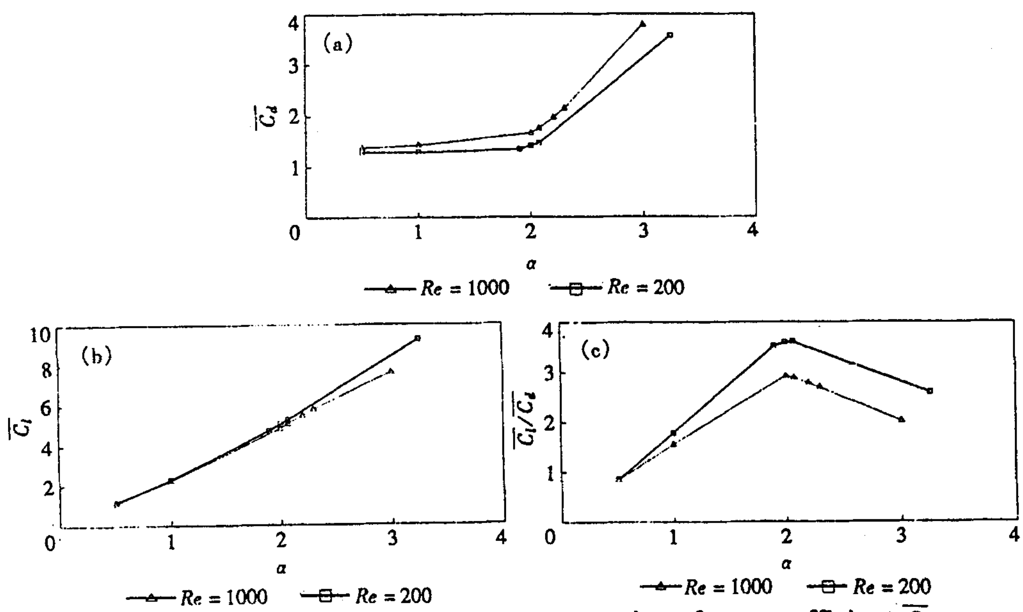

Fig. 5 The variations of (a) the mean drag force coefficient $\overline{C_d}$, (b) the mean lift force coefficient $\overline{C_l}$, (c) the mean lift to drag force ratio $\overline{C_l}/\overline{C_d}$ with a for Re=1000, 200。

streamline is flat and smooth. Besides a vortex attached with the upper side, there are not any other vortices shed from the cylinder. It is agreed with [1] and [3]'s experimental and [7]'s numerical results.

There should exist a transition state, so called the critical state, between the state of periodical alternate double side shedding vortex pattern for smaller a and the state of steady single side attached vortex pattern for larger a. So far it is little known that about the flow characters and vortex patterns at critical states. Through numerical tests, the critical speed ratio a_c are found to be 2.2 and 2.0 for Re = 1000, 200 respectively, and the characters about the vortex patterns at critical states are given for the first time. Fig. 4 is of the vorticity contours at critical states for (a) Re = 1000, a = 2.2 and (b) Re = 200, a = 2. The strength of the vortex shed from the lower side is so decreased that the vortex doesn't need to be shown in the plot. But the lower side vortex still exists, which is playing a periodical effect on the upper side vortex. So after the first main vortex is shed, the upper side vortex takes a shape like a lotus root, (not the flat and smooth shape as in the steady case). As time is developing, the parts of the 'lotus root' will shed one after one. This is like the case of single side shedding vortex of [5], but it now takes place at the critical state, and not at the steady state.

The speed ratio a also has great influence on the drag and lift force cofficients. In Fig. 5 the variations of (a) the mean drag force coefficient $\overline{C_d}$, (b) the mean lift force coefficient $\overline{C_l}$ and (c) the mean lift to drag force ratio $\overline{C_l}/\overline{C_d}$ with a are shown. The $\overline{C_l}$ increases almost linearly with increasing a. The $\overline{C_d}$ also increases with increasing a, but the increase speed before or after the critical state is different, the latter is greater than the former. So the $\overline{C_l}/\overline{C_d}$ may get a maximum value at one a. The calculated results show that the maximum $\overline{C_l}/\overline{C_d}$ will be obtained nearby the critical state. It implicates the importance of studying the critical state of a rotating circular cylinder for the flow control problems.

V. Conclusions

1. For the large broad band sparse matrix equations deduced from high order implicit difference algorithms, an efficient preconditioned conjugate gradient method, e.g. MILU-CG method is recommended to be the solver.

2. The speed ratio a plays a determining effect on the vortex patterns in the wake of a cylinder, and the variations of the drag and lift force coefficients.

3. There exists a critical state. When $\alpha < \alpha_c$, a periodical alternate double side shedding vortex pattern occurs in the wake. When $\alpha > \alpha_c$, a steady single side attached vortex pattern occurs. When $\alpha \approx \alpha_c$, a lotus-root-like single side shedding vortex pattern occurs.

4. The maximum lift to drag force ratio is obtained nearby the critical state.

References

[1] M. Coutanceau and C. Menard, Influence of rotation on the near-wake development behind an impulsively started circular cylinder, *J. Fluid Mech.*, **158** (1985), 399~446.

[2] H. M. Badr and S. C. R. Dennis, Time-dependent viscous flow past an impulsively started rotating and translating circular cylinder, *J. Fluid Mech.*, **158** (1985), 447~488.

[3] H. M. Badr, M. Coutanceau and S. C. R. Dennis, et al., Unsteady flow past a rotating circular cylinder at Reynolds numbers 10^3 and 10^4, *J. Fluid Mech.*, **220** (1990), 459~484.

[4] C. C. Chang and R. L. Chern, Vortex shedding from an impulsively started rotating and translating circular cylinder, *J. Fluid Mech.*, **233** (1991), 265~298.

[5] Y. M. Chen, Y. R. Ou and A. J. Pearlstein, Development to the wake behind a circular cylinder impulsively started into rotating and rectilinear motion, *J. Fluid Mech.*, **253** (1993), 449~484.

[6] Y. R. Ou, Mathematical modeling and numerical simulation in external flow control, *Flow Control*, Springer-Verlag (1995), 219~255.

[7] Y. T. Chew, M. Cheng and S. C. Luo, A numerical study of flow past a rotating circular cylinder using a hybrid vortex scheme, *J. Fluid Mech.*, **299** (1995), 35~71.

[8] Ling Guocan, Ling Guoping and Wang Yunping, Domain decomposition hybrid method for numerical simulation of bluff body flows, *Science in China* (*Series A*), **35**, 8 (1992), 977~990.

[9] Ling Guocan, Ling Guoping and Gu Qiyang, A new numerical method for computing the separated flow around a bluff body at high Reynolds number, *J. Huazhong Univ. Sci. Tech.*, **20**, 4 (1992), 87~93. (in Chinese)

[10] Ling Guoping and Ling Guocan, A numerical study of the vortex motion in oscillating flow around a circular cylinder at low and middle *Kc* numbers, *Acta Mechanica Sinica*, **10**, 3 (1994), 212~219.

[11] Lü Tao, T. M. Shih and C. B. Liem, *Domain Decomposition Method*, Sciece Press, Beijing (1992), 120~143. (in Chinese)

[12] T. M. Shih, C. B. Liem and X. Y. Yue, The application of MILU-CG method to three dimensional and three phase black oil model simulations, *Petroleum Exploration and Development*, **21**, 6 (1994), 52~58. (in Chinese)